Impact of surface turbulent fluxes on the formation of convective rolls in a Mediterranean windstorm

Wahiba Lfarh[1], Florian Pantillon[1], and Jean-Pierre Chaboureau[1]

[1]Laboratoire d'Aérologie, Université de Toulouse, CNRS, UPS, Toulouse, France

Key Points:

- Large eddy simulations reveal the existence of convective rolls transporting strong winds to the surface in a Mediterranean windstorm
- The inclusion of spray in surface fluxes results in a 30% reduction in the size of convective rolls and a 40% increase in momentum transport
- The results may constrain the representation of turbulent fluxes at the air-sea interface, which is uncertain under strong wind conditions

Corresponding author: Wahiba Lfarh, wahiba.lfarh@aero.obs-mip.fr

Abstract

Convective rolls contribute largely to the exchange of momentum, sensible heat and moisture in the boundary layer. They have been shown to reinforce air-sea interaction under strong wind conditions. This raises the question of how surface turbulent fluxes can, in turn, affect the rolls. Representing the air-sea exchanges during extreme wind conditions is a major challenge in weather prediction and can lead to large uncertainties in surface wind speed. The sensitivity of rolls to different representations of surface fluxes is investigated using Large Eddy Simulations. The study focuses on the Mediterranean windstorm Adrian, where convective rolls resulting from thermal and dynamical instabilities are responsible for the transport of strong winds to the surface. Considering sea spray in the parameterization of surface fluxes significantly influences roll morphology. Sea spray increases heat fluxes and favors convection. With this more pronounced thermal instability, the rolls are 30% narrower and extend over a greater height, and the downward transport of momentum is intensified by 40%, resulting in higher wind speeds at the surface. Convective rolls vanish within a few minutes in the absence of momentum fluxes, which maintain the wind shear necessary for their organization. They also quickly weaken without sensible heat fluxes, which feed the thermal instability required for their development, while latent heat fluxes play minor role. These findings emphasize the necessity of precisely representing the processes occurring at the air-sea interface, as they not only affect the thermodynamic surface conditions but also the vertical transport of momentum within the windstorm.

Plain Language Summary

Convective rolls are coherent and organized swirls that are often observed in the atmospheric boundary layer. Here, they are simulated with fine resolution in a numerical model for a Mediterranean windstorm, where they carry strong winds through the boundary layer towards the surface. Their existence requires two elements: significant exchange of both heat and momentum between the sea and the atmosphere. The morphology of convective rolls is highly dependent on air-sea exchanges, which representation in numerical models is uncertain under strong wind conditions. In particular, the evaporation of water droplets ejected by wind action on the waves may reinforce heat exchanges. When this effect is taken into account, the rolls are stronger, taller and narrower. Consequently, the wind speed increases near the surface. These findings highlight the need to better understand the interactions at the air-sea interface under windstorm conditions, because they act on the formation of damaging winds.

1 Introduction

In late October 2018, a mid-tropospheric trough formed over the eastern Atlantic, extending from Scandinavian to the Iberian Peninsula. At the surface, a broad cyclonic area developed over the western Mediterranean, to the east of the trough axis. On October 29, the strongly baroclinic environment led to the formation of windstorm Adrian (also known as Vaia) (Cavaleri et al., 2019; Davolio et al., 2020; Giovannini et al., 2021). Owing to a strong contrast between the cold air and the warm sea surface, the low-pressure system rapidly intensified and reached a minimum pressure of 977 hPa as it moved between Corsica and northwest Italy. In Corsica, Adrian caused wind gusts of up to 180 km h^{-1}, resulting in extensive damage to infrastructure and considerable economic losses.

Recent research reveals that the strong winds of windstorm Adrian have their origin from a mesoscale cold conveyor belt, which refers to a cold air flow in the lower levels of the troposphere (Lfarh et al., 2023). The fine-scale processes lead-

ing to the downward transport of strong winds were examined using a Large Eddy Simulation (LES), for which the strong winds are located in a convective boundary layer. The phase of maximum intensity of Adrian is marked by a combination of thermal instability resulting from a strong air-sea temperature contrast, and dynamic instability due to strong vertical wind shear. Such thermodynamic conditions foster the formation of convective rolls in the boundary layer.

Convective rolls are defined as quasi-two-dimensional vortices, oriented in the wind direction, creating alternating upward and downward air motions (Etling & Brown, 1993). These structures are also observed in different meteorological conditions from those of Mediterranean windstorms, such as cold-air outbreak events (Gryschka & Raasch, 2005; Chen et al., 2019) and hurricanes (Foster, 2005; Li et al., 2021). Convective rolls are known for transporting momentum, heat and moisture through their descending and ascending branches between the top of the boundary layer and the sea surface (Weckwerth et al., 1999). Previous studies have shown that convective rolls contribute half, or even much more, of the total momentum flux in hurricanes, and can reinforce air-sea interactions (Morrison et al., 2005). In Adrian, the wind is stronger along downward branch of the rolls due to higher momentum air transport from the cold conveyor belt (Lfarh et al., 2023).

The transport of momentum, heat and moisture by convective rolls in the boundary layer could influence surface fluxes. This raises the question of how these fluxes in turn affect the characteristics of the rolls. Exchanges at the air-sea interface strongly influence the thermodynamic conditions of the atmosphere. Heat fluxes, in particular, are among the diabatic processes involved in the development of extra-tropical cyclones. Previous studies have shown that the release of latent heat during condensation processes can strengthen vorticity at lower levels, and therefore contribute to the cyclogenesis (Booth et al., 2012; Ludwig et al., 2014). As well as their mesoscale impact, air-sea interactions play a significant role in modulating surface wind speeds during windstorms. Schultz and Sienkiewicz (2013) suggested that heat fluxes promote shallow convection and facilitate wind mixing from the upper boundary layer towards the surface.

Turbulent fluxes at the air-sea interface occur on spatial and temporal scales too small to be explicitly resolved in numerical weather prediction models, and are therefore parameterized. The importance of air-sea interactions has led to widespread interest in improving their representation in numerical weather prediction systems (Lewis et al., 2019). To date, many uncertainties persist in flux measurements at the air-sea interface, particularly in high wind situations. Flux measurements are limited to a wind speed of about 20 m s^{-1}. This may explain the underestimation of near-surface wind speed in windstorms compared to in situ and satellite observations (Pineau-Guillou et al., 2018). Although direct measurements from ocean buoys, GPS dropsondes and airborne radar can be employed to quantify surface fluxes under strong wind conditions, the scarcity of such observations presents major challenges for model validation (Richter & Stern, 2014; Zou et al., 2018). In addition, the air-sea interface becomes more complex under strong wind conditions, with the presence of foam and sea spray resulting from breaking waves. These factors make measuring and modeling turbulent fluxes all the more difficult (Emanuel, 2003; Sroka & Emanuel, 2021).

Theoretical studies and numerical simulations have shown that the microphysical processes governing the generation and evaporation of sea spray can have a significant impact on air-sea exchanges. In strong winds, breaking waves at the air-sea interface can produce large quantities of spray droplets. As they float in the air, spray droplets carry a large amount of energy due to their speed and abundance, generating more intense momentum fluxes (Veron et al., 2012; Sroka & Emanuel, 2022). In addition, sea spray has the effect of cooling the air and transferring latent

heat to the atmosphere when it evaporates, creating favorable conditions for more powerful heat exchange between the sea surface and the atmosphere (Andreas et al., 2015; Jeong et al., 2012). Using a coupled ocean-wave-atmosphere model, Zhao et al. (2017) found that sea spray caused an increase in cyclone intensity by strengthening air-sea fluxes. Sroka and Emanuel (2021) concluded that the inclusion of sea spray in turbulent flux parameterizations is crucial in extreme wind situations.

The Mediterranean is an ideal test-bed for investigating these complex surface processes under strong wind situations. Regional winds bring cold, dry continental air over the warm waters of the Mediterranean, leading to intense air-sea interactions (Flamant, 2003). In this cyclogenesis-prone region, low-pressure systems are not only maintained, but also reinforced by exchanges resulting from variations in temperature and humidity between the atmosphere and the sea (Jansà et al., 1994). Unlike tropical cyclones and Atlantic windstorms, there are few studies devoted to the role of surface turbulent fluxes in the mesoscale dynamics of Mediterranean windstorms. Furthermore, the impact of these fluxes on fine-scale processes is largely unknown for extra-tropical cyclones. The main objective of this study is to examine how turbulent fluxes at the air-sea interface affect the formation and organization of convective rolls and, hence, surface winds during the Mediterranean windstorm Adrian. To achieve this purpose, sensitivity tests to different parameterizations of turbulent fluxes are carried out using LES.

The paper is structured as follows: Section 2 briefly presents the modeling strategy, the parameterizations used to calculate turbulent fluxes and the analysis tools. Section 3 examines the influence of turbulent fluxes at the mesoscale, particularly on changes in the trajectory and intensity of the windstorm. Section 4 investigates the effects of parameterizations on fine scale convective rolls and surface winds before discussing the impact of each turbulent flux independently of the others. Finally, section 5 summarizes the main results.

2 Methods

2.1 Numerical configuration and sensitivity experiments

Two reference simulations, a mesoscale one and the other a LES, are carried out with the Meso-NH non-hydrostatic atmospheric model (Lac et al., 2018) to study the strong mesoscale winds in windstorm Adrian and the fine-scale processes responsible for their transport to the surface, respectively. Both simulations share the same vertical grid with 72 levels reaching 22 km and a finer grid spacing near the surface (10 m at the first level). They are initialized at 0600 UTC on October 29, 2018 from the operational analysis of the European Centre for Medium-Range Weather Forecasts (ECMWF) and run for 15 h.

The mesoscale simulation covers a domain centered on the western Mediterranean (domain D1 in Figure 1a) with a horizontal grid spacing of 1000 m allowing explicit representation of deep convection. The LES is nested in the mesoscale simulation using a one-way nested method. It has a horizontal grid spacing of 200 m over a large domain covering part of the Mediterranean Sea and the whole of Corsica (domain D2 in Figure 1b). Both simulations are based on the same parameterization schemes, except for three. The mesoscale simulation uses the fifth-order WENO (weighted essentially non-oscillatory) advection scheme for momentum variables (Shu & Osher, 1988), the EDMF (eddy-diffusivity mass flux) parametrization of Pergaud et al. (2009) for shallow convection, and the 1D version of the scheme of Cuxart et al. (2000) for turbulence. In the LES, the EDMF parameterization is deactivated, as convection is explicitly represented, and a more accurate fourth-order centered advection scheme is used along with a 3D version of the turbulence scheme.

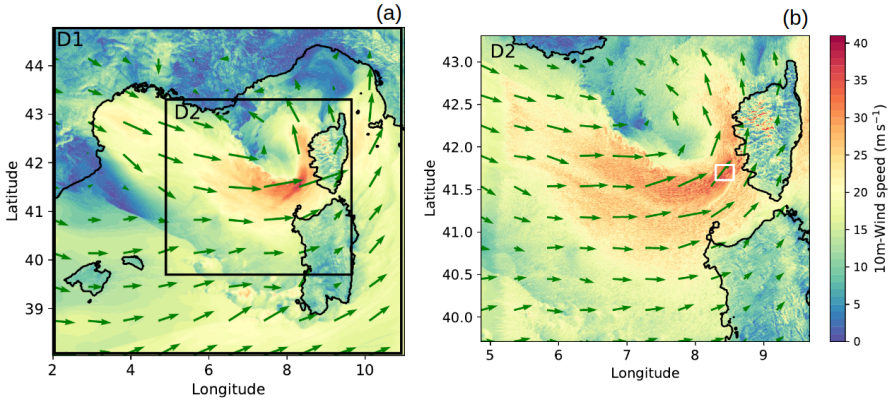

Figure 1: Wind speeds at 10 m height at 1530 UTC, from reference simulations at 1000 m (a) and 200 m (b) horizontal resolution. The black squares represent the D1 and D2 domains in(a). The wind direction at 10 m is represented by the green arrows. In (b), the white square indicates the zoomed-in area of 20 by 20 km shown in Figure 5.

For further details on the simulation configuration, the reader is referred to Lfarh et al. (2023).

Sensitivity experiments to turbulent fluxes at the air-sea interface are carried out at both scales based on the two reference simulations. In order to assess the impact of turbulent flux parameterizations on the evolution of the Adrian storm at mesoscale, a first series of sensitivity experiments are performed with a horizontal grid spacing of 1000 m on the D1 domain. These simulations are initialized at 1200 UTC from the reference simulation and run for 6 h, including the development and intensification phase of windstorm Adrian. To shed light on the impact of turbulent exchanges between the air and the sea on the convective rolls that bring strong winds to the surface, a second series of sensitivity experiments is performed at a horizontal resolution of 200 m on the D2 domain. These experiments are also initialized from the reference simulations and conducted over a short period from 1500 UTC to 1530 UTC, when the windstorm reached its maximum intensity.

Surface-atmosphere interactions are managed by a surface modeling platform called SURFEX (Surface Externalised), which is coupled to Meso-NH (Masson et al., 2013). This platform integrates several physical models that deal with the different characteristics of the surface of the Earth. In reference simulations, turbulent air-sea exchanges are represented by default using the COARE3 (Coupled Ocean-Atmosphere Response Experiment) parameterization (Fairall et al., 2003). Other parameterizations of air-sea exchanges widely used are tested at both 1000 m and 200 m resolutions and are described hereinafter. In addition to the different parameterizations, three other sensitivity experiments to momentum and heat fluxes are performed in this study. The aim is to isolate the impact of each type of fluxes on convective rolls and surface winds. Using the COARE3 reference parameterization, the NoM, NoH and NoLE simulations are performed at a horizontal resolution of 200 m, with momentum, sensible heat and latent heat fluxes set to zero, respectively. The simulations are labelled according to the name of the parameterization used, followed by "1" and "2" to refer to the horizontal resolutions of 1000 and 200 m. The model configuration for each simulation is summarized in Table 1.

Table 1: Configuration of air-sea turbulent flux sensitivity experiments including the main parameterization schemes used.

Simulation	Grid mesh (m)	Advection	Shallow convection	Turbulence	Air-Sea fluxes
Coare1	1000	WENO	Yes	1D	COARE
Andreas1	1000	WENO	Yes	1D	ANDREAS
Ecume1	1000	WENO	Yes	1D	ECUME6
Wasp1	1000	WENO	Yes	1D	WASP
Coare2	200	CEN4TH	No	3D	COARE
Andreas2	200	CEN4TH	No	3D	ANDREAS
Ecume2	200	CEN4TH	No	3D	ECUME6
Wasp2	200	CEN4TH	No	3D	WASP
NoM	200	CEN4TH	No	3D	No momentum fluxes
NoH	200	CEN4TH	No	3D	No sensible heat fluxes
NoLE	200	CEN4TH	No	3D	No latent heat fluxes

2.2 Parameterizations of turbulent fluxes at the air-sea interface

Parameterizing turbulent fluxes consists in defining a formulation of turbulent fluctuations close to the surface. The formulation takes into account all processes at the air-sea interface that can impact the fluctuations, such as waves, sea spray, etc. Air-sea fluxes are calculated on the basis of the Monin and Obukhov (1957) similarity theory, enabling the estimation of fluxes generated by complex turbulent processes in the boundary layer as a function of mean model parameters. These parameters are based on global or bulk aerodynamic algorithms (Liu et al., 1979). The parameterizations calculate turbulent fluxes as follows:

$$\begin{aligned} \tau_{\text{bulk}} &= \rho\overline{w'u'} = -\rho u_*^2 \\ H_{\text{bulk}} &= \rho c_p\overline{w'\theta'} = -\rho c_p u_*\theta_* \\ LE_{\text{bulk}} &= \rho L_v\overline{w'q'} = -\rho L_v u_* q_* \end{aligned} \tag{1}$$

where τ is the momentum flux, H the sensible heat flux and LE the latent heat flux. ρ is the air surface density, c_p the heat capacity of air at constant pressure and L_v the latent heat of vaporization. u_*, θ_* and q_* are scaling parameters for momentum, potential temperature and humidity, respectively. Bulk algorithms are based on the determination of constants called exchange coefficients (or aerodynamic coefficients), which establish a relationship between turbulent fluxes and mean parameters. Turbulent fluxes are defined as a function of vertical gradients of wind speed ΔU, potential temperature $\Delta\theta$ and humidity Δq, with C_D, C_H and C_E the exchange coefficients for momentum, sensible heat and latent heat, respectively :

$$\begin{aligned} \tau = & \quad -\rho C_D\Delta U^2 = & -\rho C_D(U_a - U_s)^2 \\ H = & \quad -\rho c_p C_H\Delta U\Delta\theta = & -\rho c_p C_H(U_a - U_s)(\theta_a - \theta_s) \\ LE = & \quad -\rho L_v C_E\Delta U\Delta q = & -\rho L_v C_E(U_a - U_s)(q_a - q_s) \end{aligned} \tag{2}$$

where the a index corresponds to the first atmospheric level, and the s index to the sea surface.

Even though all parametrizations are based on the same theory, they differ from one another. Each parametrization uses its own stability function and closure assumption, allowing simplified consideration of complex variations in the near-surface atmosphere. The formulations of turbulent flux parametrizations differ in

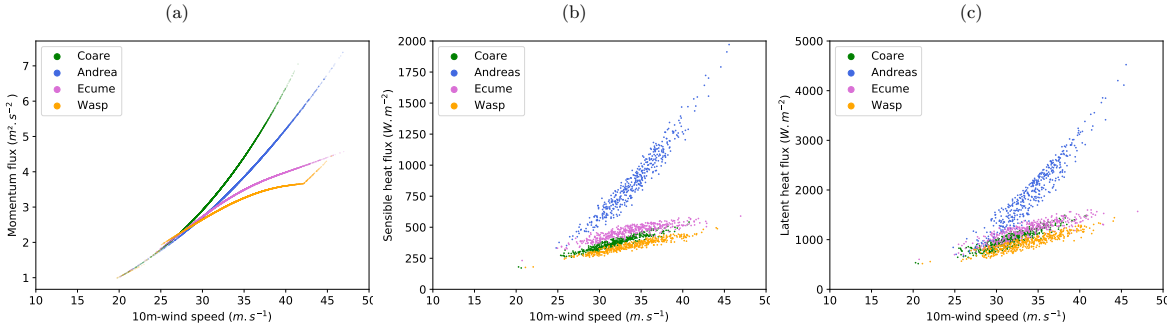

Figure 2: Turbulent fluxes of (a) momentum, (b) sensible and (c) latent heat as a function of wind speed at 10 m from the Coare2 (green), Andreas2 (blue), Ecume2 (pink) and Wasp2 (orange) simulations at 1530 UTC. Turbulent fluxes are calculated at each grid point on the zoom represented by the white square on Figure 1b.

their expressions of exchange coefficients and roughness length calculations, and also in the way they do or do not take into account the effects of specific physical processes (Brunke et al., 2003). In this article, four well-established parameterizations are used: COARE3.0 (Fairall et al., 2003), ANDREAS (Andreas et al., 2015), ECUME6, the sixth version of Exchange Coefficient Unified Multi-campaign Experiments used operationally by Météo-France (Belamari, 2005), and WASP (Wave-Age Stress dependant Parametrization) (Sauvage et al., 2020). They are detailed in Appendix A.

Differences between parameterizations are illustrated at 1530 UTC, when wind speeds reaching 40 m s^{-1} occur in a narrow belt along the south flank of the low-pressure center (white square in Figure 1b). The momentum, sensible and latent heat fluxes are represented in Figure 2 as a function of wind speed at 10 m. For all four parametrizations, momentum fluxes show a similar increase with wind speed for speeds below 30 m s^{-1} (Figure 2a). At speeds above 30 m s^{-1}, they diverge depending on the parameterization used. The strongest momentum fluxes are produced by the COARE and ANDREAS parametrizations. In contrast, ECUME and WASP show a relatively similar evolution under strong wind conditions, characterized by lower fluxes of momentum, with a tendency to saturation at speeds above 30 m s^{-1}. This contrast shows the impact of accounting or not for the saturation of the drag coefficient when wind speed exceeds 30 m s^{-1}. The differences between sensible and latent heat flux parameterizations become apparent at speeds of 20 m s^{-1} and above. The COARE, ECUME and WASP parametrizations show similar heat fluxes at high speeds, varying between 200 and 500 W m^{-2} for sensible heat fluxes, and between 500 and 1500 W m^{-2} for latent heat fluxes. ANDREAS reveals large deviations for wind speeds in excess of 20 m s^{-1}, illustrating the impact of the sea spray included in the parametrization. This translates into fluxes in excess of 2000 W m^{-2} and 4000 W m^{-2} for sensible and latent heat respectively, at wind speeds in excess of 45 m s^{-1}.

2.3 Auto-correlation function

As in Lfarh et al. (2023) fine-scale wind speed structures associated with the Adrian storm are characterized using the spatial auto-correlation function (ACF). The ACF is a statistical approach commonly used to assess the spatial variability of turbulence organization in the atmospheric boundary layer, defining the main shape, direction and characteristic size of structures (Lohou et al., 1998; Brilouet et

al., 2023). In practice, ACF measures the correlation of a variable with itself at spatial positions shifted along the x and y directions. In this case study, the 2D ACF $R_F(\delta_x, \delta_y)$ is calculated from the vertical wind speed fields $F(x, y)$ at lags δ_x and δ_y, using the method of Granero Belinchon et al. (2022) as follows:

$$R_F(\delta_x, \delta_y) = \langle F(x, y) \times F(x + \delta_x, y + \delta_y) \rangle \tag{3}$$

where $F(x, y)$ is the field value at position (x,y), $F(x+\delta_x, y+\delta_y)$ is the field value at a position lagged by (δ_x,δ_y) from (x,y) and $\langle ... \rangle$ denotes the spatial average.

The first step is to extract the main shape of the structures, which can be either elliptical, suggesting the presence of convective rolls, or circular, as in the case of convective cells. The analysis is based on the integral length L_{es}, defined as the integral of the ACF where the field $F(x, y)$ remains correlated with itself. L_{es} is calculated in different directions to detect possible anisotropy (Lohou et al., 2000). The geometry of the structures can be determined by fitting the set of points corresponding to L_{es}. An elliptical fit indicates an elongated, elliptical structure, while a circular fit suggests a circular structure. In a second step, the geometric parameters of the structure are determined, including the major axis r_a and the minor axis r_b. These two axes are used to quantify the flatness parameter f calculated as follows:

$$f = \frac{r_a - r_b}{r_a} \tag{4}$$

where r_a and r_b are the major and minor radii of the structure, respectively. This parameter is used to distinguish the roll structures, where f tends towards 1, from the cellular structures, where the parameter tends towards 0. The third step is to estimate the length scale of the organized structure L_{os}, which represents its characteristic size. This length is defined as the distance between two correlation maxima in the ACF.

3 Impact of surface fluxes on the mesoscale dynamics

The effects of the four parameterizations are assessed here on the evolution of windstorm Adrian at mesoscale. On the morning of October 29, 2018, a large low-pressure system intensified into windstorm Adrian in the western Mediterranean as a result of baroclinic interaction. The observed (best-track) and simulated trajectories from the Coare1, Andreas1, Ecume1 and Wasp1 simulations are shown over the D2 domain from 1200 to 1700 UTC (Figure 3a), until the cyclone moves out of the domain and arrives on land. At 1200 UTC, Adrian is located to the west of Sardinia, then moves northwards along a meridional trajectory. It approaches Corsica between 1500 and 1600 UTC. All simulated trajectories remain close to the best track, demonstrating the ability of the model to capture the trajectory of Adrian. Furthermore, the simulated trajectories remain close to each other despite slight positional shifts. This suggests that the track of Adrian over this short period does not depend much on the air-sea flux parameterization used, but is mainly determined by the baroclinic interaction.

Temporal evolutions of mean sea level pressure (MSLP) and 99th percentile wind speeds at 10 m over the sea are calculated from 1200 to 1800 on the D2 domain (Figures 3b and 3c). The evolution of pressure indicates that Adrian intensified rapidly, reaching its maximum intensity between 1500 and 1600 UTC, i.e.,

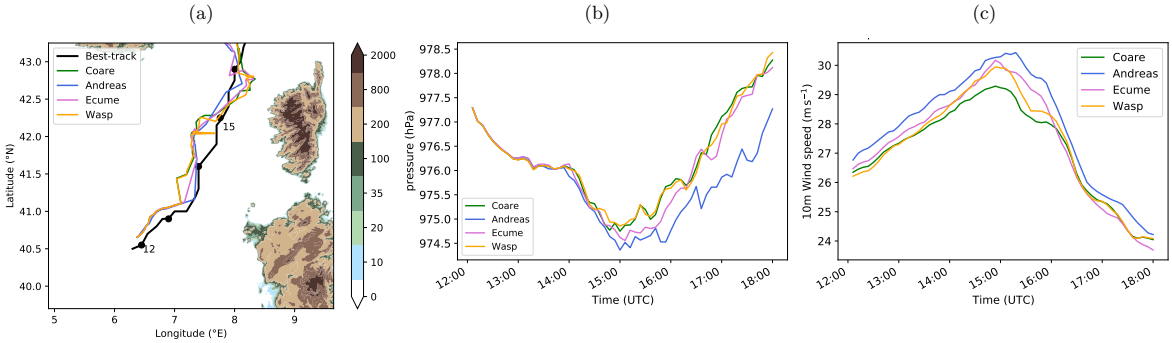

Figure 3: (a) Trajectories of Adrian as observed (black line) and simulated by Coare1, Andreas1, Ecume1 and Wasp1 (colored lines) every 15 min between 1200 and 1700 UTC. The black circular markers indicate the position observed every hour. Terrain height is shown in color. The best observed track is estimated from the center of the cyclonic cloud roll-up on the Spinning Enhanced Visible and InfraRed Imager (SEVIRI) High Resolution Visible (HRV) satellite image, while simulated trajectories are estimated from the position of the lowest mean sea-level pressure. (b) Temporal evolution of minimum pressure at sea level and (c) 99th percentile wind speed at 10 m over sea. The evolutions are calculated over the sea part of the D2 domain between 1200 and 1800 UTC.

975 hPa in Coare1 (Figure 3b). Sensitivity tests in LES are performed during this period, and in the following section, figures will be presented at 1530 UTC. The MSLP begins to rise gradually from 1600 UTC, indicating the beginning of the weakening of Adrian. During the first two hours of pressure evolution, all simulations show a similar tendency. The differences become perceptible from the moment of maximum intensity of the depression. The Ecume1 and Wasp1 simulations show a similar evolution to that of Coare1, despite a slightly more pronounced deepening in Ecume1. Andreas1 shows a distinct evolution and a deeper depression. The pressure difference with the reference simulation does not exceed 0.5 hPa between 1500 and 1600 UTC, but reaches 1.5 hPa at 1800 UTC.

In the early afternoon, wind speeds exceed 25 m s^{-1} due to the intensification of the low-pressure system and increase rapidly to reach a peak at around 1500 UTC, with 99th percentile values of 29 m s^{-1} for Coare1 (Figure 3c). As Adrian weakens, wind speeds gradually decrease until 1800 UTC. Unlike the MSLP, wind speed evolutions show immediate differences at the start of the simulations, becoming more noticeable during the maximum intensification of the depression. The difference reaches 1 m s^{-1} in Ecume1 and Wasp1 compared with Coare1, and rises to 2 m s^{-1} in Andreas1. The intensity differences obtained with the ANDREAS parametrization are consistent with the results of Perrie et al. (2005) and Zhang2006, who found that including sea spray in the surface fluxes leads to a decrease in surface pressure during windstorms by a few hPa and an increase in surface wind speed by a few m s^{-1}. Moreover, as in the case of Adrian, the authors found that sea spray has a minor effect on the windstorm trajectory. As saturation of the drag coefficient is not taken into account in the COARE parameterization, it is not surprising that the Coare1 simulation produces the lowest wind speeds compared with the other simulations. After 1600 UTC, the differences become negligible and reflect an almost identical evolution of wind speeds.

Due to the passage of Adrian near Corsica, stations recorded high wind speeds, particularly in the western and northern coastal stations, where measurements exceeded 30 m s^{-1} (Figure 4a). To assess the impact of the parameterizations on

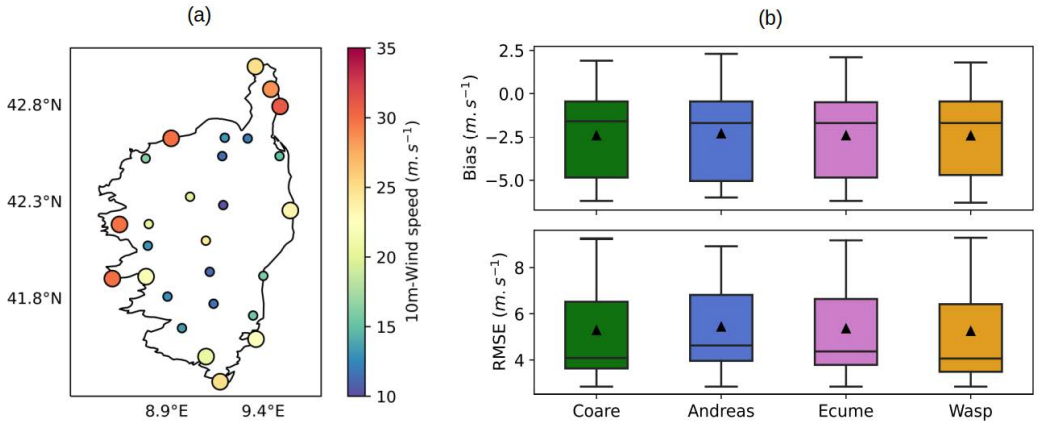

Figure 4: (a) Maximum wind speed at 10 m observed between 1200 and 1800 UTC at stations in Corsica. Markers with large circles correspond to coastal stations recording wind speeds exceeding 20 m s^{-1}. (b) Box plots of the bias and root-mean-square error (RMSE) between simulated and observed wind speeds at the 11 coastal stations, calculated over a period from 1200 to 1800 UTC every 6 min. Boxes represent simulations Coare1, Andreas1, Ecume1 and Wasp1 in green, blue, pink and orange colors, respectively.

the capacity of the model to reproduce the observations, a comparative analysis of the different turbulent fluxes parametrizations is performed on 11 coastal stations (markers with large circles on Figure 4a). These 11 stations are selected on the basis of two criteria: proximity to the sea and wind speeds exceeding the critical threshold of 20 m s^{-1}, at which parameterizations begin to diverge from one another. Wind speed measurements at 10 m are recorded by the Météo-France surface weather network at 6-min intervals. To ensure a fair comparison, instantaneous wind speeds from the sensitivity tests are also averaged over a 6-min period, from 1200 to 1800 UTC. For the 11 stations, the simulations show a median bias of around -1.7 m s^{-1}, indicating a small underestimation of observed wind speeds. Minor differences are noted in root-mean-square error (RMSE). The median RMSE values are 4.09, 4.93, 4.37 and 4.06 m s^{-1} for Coare1, Andreas1, Ecume1 and Wasp1, respectively (Figure 3b). These results suggest that simulations are somewhat more realistic with the COARE and WASP parameterizations and slightly less with ANDREAS compared to ECUME.

In conclusion, the four simulations reproduce station observations in a similar way, demonstrating that turbulent fluxes at the air-sea interface have little impact on wind speed over land. Over the short 6-h period, the trajectory of the windstorm is unaffected by the choice of surface flux parameterization. This confirms that the trajectory is mainly determined by large-scale flow. Regarding the intensity of Adrian, the ANDREAS parameterization generates a more pronounced low-pressure system, resulting in slightly higher wind speeds compared to the reference simulation Coare1, due to the inclusion of sea spray. Consequently, LES sensitivity tests can be carried out over short periods to assess the impact of turbulent exchanges at the air-sea interface on convective rolls, while preserving mesoscale characteristics of the windstorm.

4 Impact of turbulent fluxes on the finescale

4.1 Morphology of convective rolls

In the following, the study focuses on a 20 km by 20 km region, representative of the narrow band of strong winds generated on the southern flank of the low-pressure center (white square in Figure 1b). Wind speeds lie above 20 m s^{-1}, a threshold at which turbulent flux parameterizations begin to diverge (Figure 2). The analysis is based on LES simulations, inspecting horizontal and vertical cross-sections of wind speeds (Figure 5). In the reference simulation Coare2, the horizontal section (Figure 5a) illustrates band-like wind structures where speeds exceed 48 m s^{-1}. The structures are approximately oriented in the wind direction from the southwest (red arrows). Horizontal sections are shown at z = 200 m, because the structures are well marked at this altitude. The vertical extent of the structures is roughly equivalent to the height of the boundary layer z_i, which reaches around 700 m (Figure 5b). A regular alternation of upward and downward velocities can be seen on vertical winds (black contours), which is a signature of rolls in the boundary layer. This result is in line with the findings of Lfarh et al. (2023), who showed that the boundary layer in strong wind regions is organized into convective rolls at 1515 UTC in windstorm Adrian. Such structures are observed throughout the narrow belt of strong winds and persist until the weakening phase of the windstorm.

The boundary layer organization in Ecume2 and Wasp2 simulations is similar to the reference simulation (Figures 5e-5h). The Andreas2 simulation stands out the most. The horizontal section shows coherent structures that are narrower than in Coare2 (Figure 5c). The upward and downward motions are more pronounced and extend over a greater vertical distance (Figure 5d). Accordingly, the boundary layer height is higher, showing marked fluctuations between 1000 and 1500 m. ntation and characteristic size of convective rolls.

The spatial characteristics of the convective rolls are examined in the four simulations using the ACF calculated from the vertical wind speed field at 1530 UTC over the zoomed area shown in Figure 5. Figure 6 presents vertical profiles of the flatness parameter, orie

According to Brilouet et al. (2023) a threshold on the flatness parameter is chosen to distinguish roll structures with $f > 0.7$ from disorganized structures with $f < 0.7$. In Coare2, the flatness parameter reveals the presence of rolls up to z=400 m and a transition into disorganized structures above (Figure 6a). The mean wind direction varies slightly with height, from 60° to 50° clockwise, while the roll direction evolves counter-clockwise from 50° to 70°. Below z=400 m, this results in rolls mainly oriented in the wind direction, with a minor difference of around 10° (Figure 6b). Accordingly, observational studies have shown that convective rolls are often aligned within 10 to 20° from the mean wind direction (Atkinson & Wu Zhang, 1996; Foster, 2005). Finally, the size of rolls can be determined up to 400 m height and reaches 2000 m mostly, giving an aspect ratio λ/z_i of 2.73. Altogether, this implies that elliptical roll structures are present below 400 m in Coare2. The morphological characteristics of the convective rolls at 1530 UTC are comparable to those found at 1515 UTC in Lfarh et al. (2023), except that the size of the rolls was slightly larger, reaching 2400 m.

In the Ecume2 and Wasp2 simulations, the size of the convective rolls vary slightly, between 2200 and 2400 m, but remain comparable to that in the reference simulation (Figure 6c). The other morphological characteristics are similar (Figure 6a, b). For Andreas2, the flatness parameter remains more constant with height, the direction of the rolls is closer to the mean wind direction and their smaller size of 1400 m is uniform over a longer vertical extent of 500 m. The aspect ratio in An-

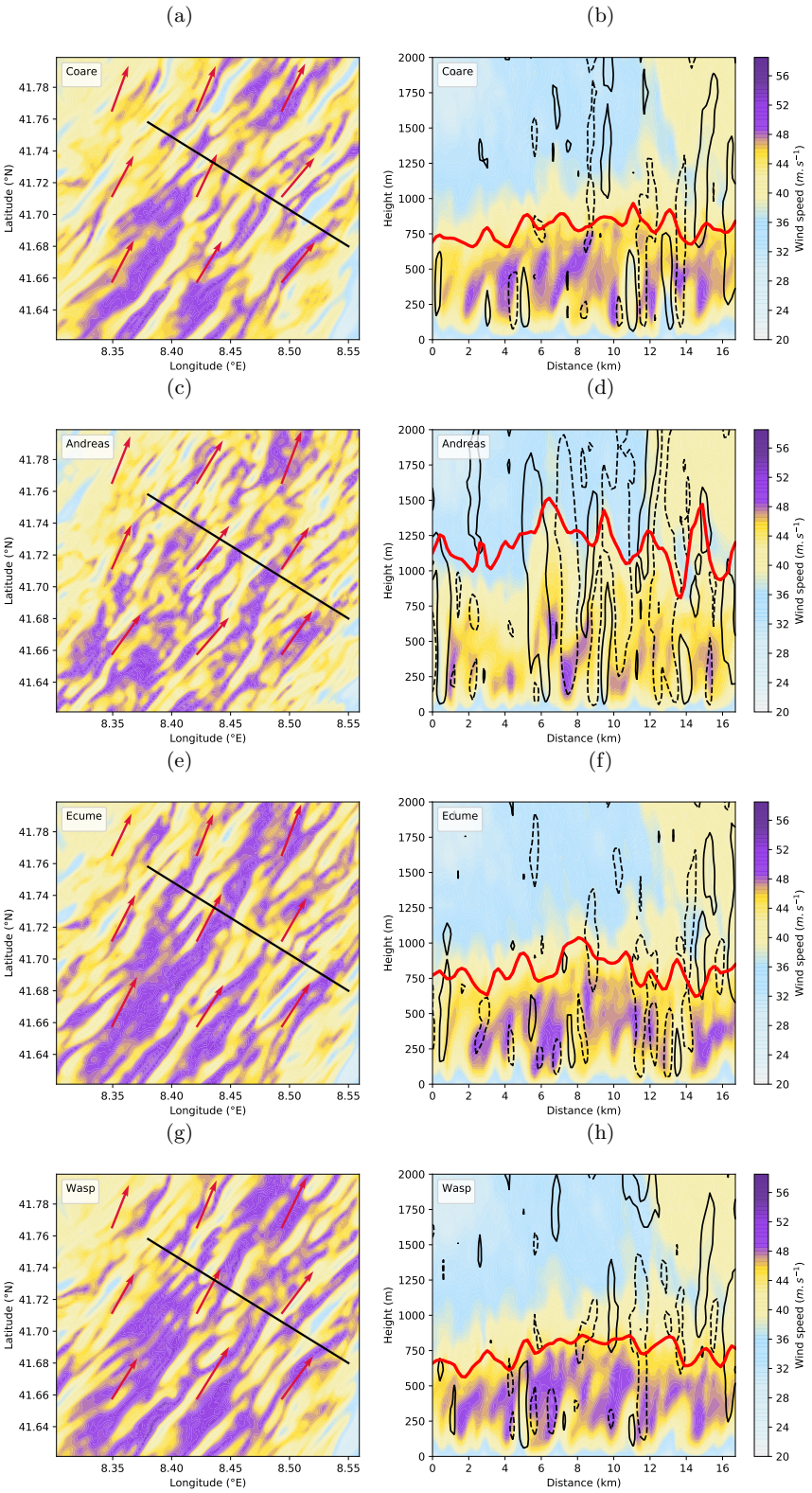

Figure 5: (left) Horizontal sections at z=200 m and (right) vertical sections of horizontal wind speed at 1530 UTC from (a, b) Coare2, (c, d) Andreas2, (e, f) Ecume2 and (g, f) Wasp2. The black lines in the horizontal sections shows the location of the vertical sections. The wind direction is shown by the red arrows. The thick red line in the vertical sections corresponds to the height of the boundary layer. Black contours indicate vertical velocity, solid lines correspond to 1 m s^{-1} and dotted lines to -1 m s^{-1}.

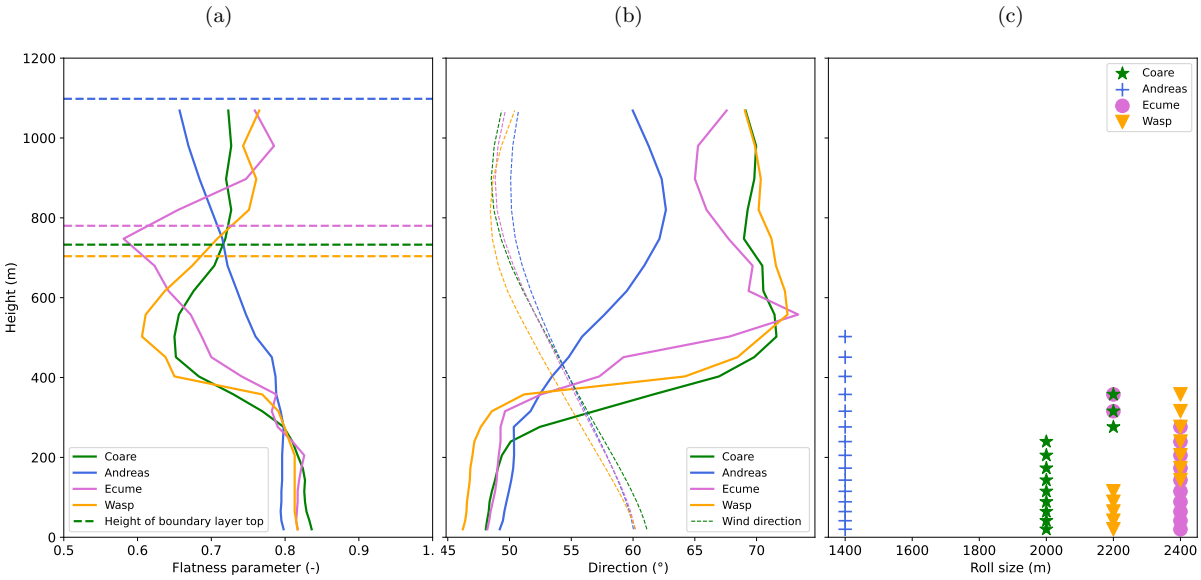

Figure 6: Vertical profiles of (a) flatness parameter f, (b) mean wind direction dotted curves) and structure direction (solide curves), (c) convective roll size identified from the auto-correlation function at 1530 UTC. Dashed lines in (a) indicate the boundary layer height averaged over the zoomed domain in Figure 5 for each simulation.

drea2 is 1.27, which indicates that the rolls are narrower in comparison to the height of the boundary layer. Table 2 summarizes the descriptive parameters of convective rolls in the different simulations. Altogether, the number of rolls over the narrow band of strong winds (distance of about 20 km) is $n \approx 10$ in Coare2, $n \approx 8$ in Ecume2 and Wasp2, and $n \approx 14$ in Andreas2.

4.2 Vertical wind transport by convective rolls

Over the same region shown in Figure 5, the wind speed increases progressively from z=1200 m downward and reaches a maximum near z=400 m, then decreases as approaching the surface (Figure 7a). Compared to the other simulations, Andreas2 shows slower winds near z=400 m and above. At the surface, the wind speed ranges from 30 m s^{-1} in Coare2 to 33 m s^{-1} in Andreas2, while values in Ecume2 and Wasp2 fall between these two extremes. In the Coare2 reference simulation, the virtual potential temperature profile shows a decrease from the surface up to an altitude of 200 m, indicating instability characterized by a warm, moist surface layer favorable to convection (Figure 7b). Ecume2 and Wasp2 show a similar profile, with slightly higher temperatures in Ecume2. The surface temperature is higher and the vertical gradient is more pronounced in Andreas2, showing a rapid decrease with altitude. This is due to the enhanced surface fluxes of sensible and latent heat, which increase air temperature and humidity.

The boundary layer stability can be assessed with the instability parameter $\zeta = - z_i/L$, where L is the length of Monin and Obukhov (1957) and represents the distance above the surface where the production of buoyancy turbulence exceeds that of shear turbulence. Previous studies revealed that in a fully convective boundary, i.e. $\zeta \gg 1$, buoyancy dominates turbulence generation throughout the boundary layer (Khanna & Brasseur, 1998; Salesky et al., 2017). The ζ values are 0.5, 1.56, 0.71 and 0.52 for Coare2, Andreas2, Ecume2 and Wasp2 respectively (Table 2).

Table 2: Descriptive parameters of the boundary layer and of convective rolls in the LES sensitivity tests.

Simulation	L (m)	z_i (m)	ζ =-z_i/L	λ	λ/z_i
Coare2	-1453	732	0.50	2000	2.73
Andreas2	-701	1098	1.56	1400	1.27
Ecume2	-1089	780	0.71	2400	3.07
Wasp2	-1331	703	0.52	2400	3.41
NoLE	-1372	692	0.50	1600	2.31
NoH	-1938793	509	0.0002	-	-
NoM	0	854	-	-	-

Therefore, as opposed to other simulations where shear dominates turbulent generation, the enhanced thermal instability by a factor 2–3 in Andreas2 means that turbulence is mostly generated by buoyancy. Furthermore, the instability parameter is widely used to predict roll convection and quantify the effects of shear and buoyancy on roll formation. The obtained values of ζ are consistent with results from Weckwerth et al. (1999), which indicate that roll structures appear for $\zeta < 10$, and with the recent study of Stopa et al. (2022), which reveals that coherent roll structures occur in a slightly unstable but nearly neutral atmosphere.

While convective rolls pilot vertical motion in the boundary layer, turbulence consisting of irregular eddies is one of the most important transport processes near the surface. This raises the question of the respective roles of convective rolls and turbulent motion in vertical momentum transport. The distinction is estimated here by the separation between resolved motion, which has been shown to consist in organized roll structures, and subgrid-scale motion represented by the turbulence scheme. This assumption likely overestimates the turbulent contribution, because convective rolls are not fully resolved with 200 m horizontal grid spacing (Lfarh et al., 2023).

In Coare2, the sum of resolved momentum fluxes and subgrid-scale momentum fluxes (solid green line in Figure 7c), which corresponds to the total momentum transport, shows a gradual strengthening with decreasing height. Resolved momentum fluxes dominate at altitudes above z≈200 m (dashed lines), while they decrease progressively toward the surface and subgrid-scale motion becomes responsible for most of the momentum transport. Vertical profiles in Ecume2 and Wasp2 remain similar to those observed in Coare2. In contrast, vertical profiles in Andreas2 reveal a clear distinction from the other simulations. The total transport is much greater both near the surface and aloft due to stronger resolved momentum fluxes, which dominate down to z≈100 m. At z=200 m, resolved fluxes are enhanced by 40% compared to the reference simulation. This enhanced downward transport in Andreas2 is consistent with the larger vertical extent of convective rolls and can explain the weaker winds in the middle boundary layer and the stronger winds near the surface compared to the other simulations (Figure 7a). Interestingly, the enhancement of vertical momentum transport by 40% in Andreas2 compared to Coare2 roughly matches the increase from n≈10 to n≈14 in the number of rolls over the narrow band of strong winds (or the decrease in their size from λ=2000 m to λ=1400 m).

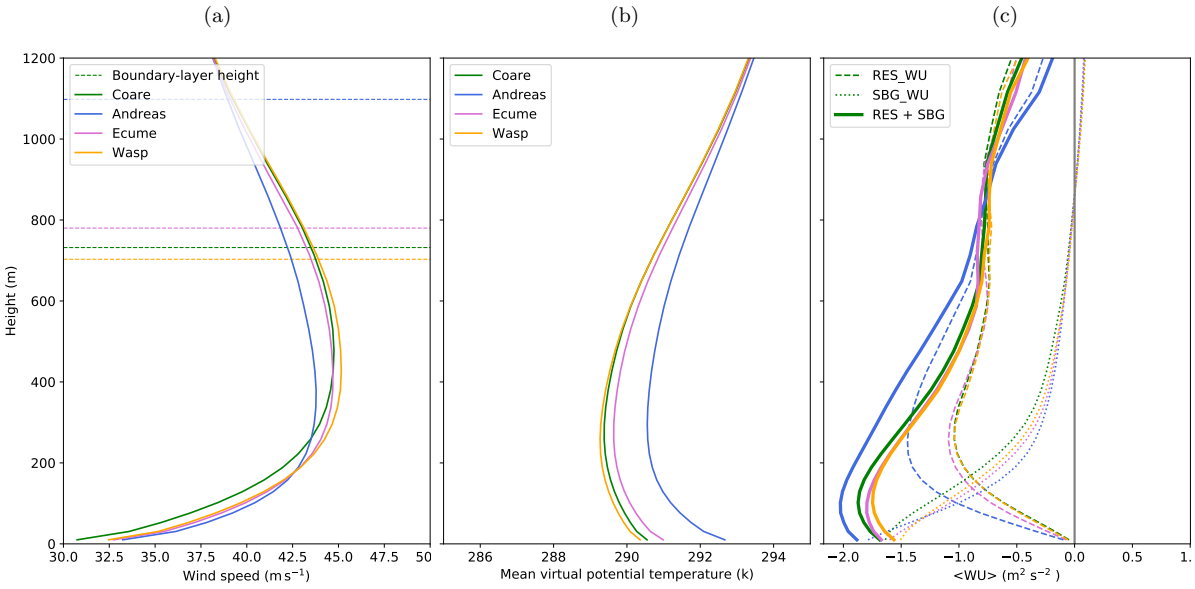

Figure 7: Vertical profile of (a) horizontal wind speed, (b) virtual potential temperature and (c) vertical fluxes of zonal momentum at 1530 UTC. The dotted horizontal lines indicate the boundary-layer height in (a). The dashed, dotted and solid lines show the resolved, subgrid and total contributions in (c). The profiles are averaged over the area shown in Figure 5.

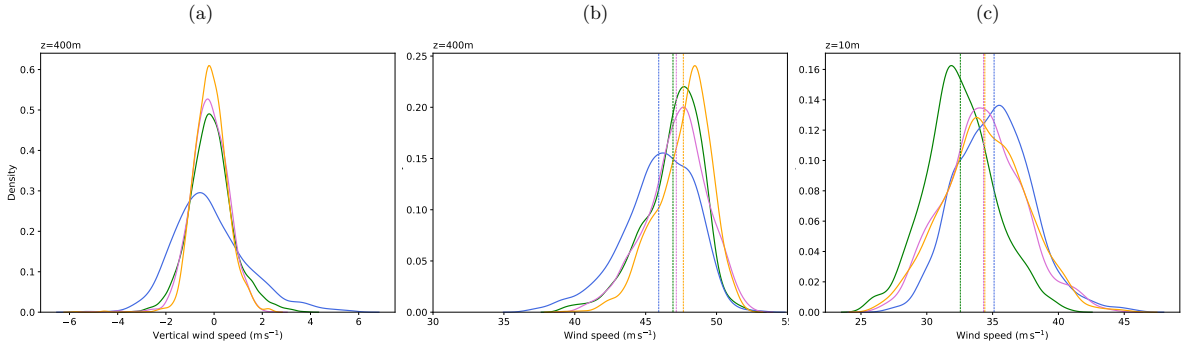

Figure 8: Probability density functions (PDFs) of (a) vertical wind speed at 400 m height and horizontal wind speed at heights (b) 400 m and (c) 10 m. The vertical lines indicate the mean values in (b, c). The PDFs are calculated over the area shown in Figure 5.

Thus, the transport of momentum per roll is equivalent between the two simulations and the smaller but more numerous rolls in Andreas2 imply a stronger total transport. In contrast, simulations Ecume2 and Wasp2 show values of resolved vertical momentum transport similar to Coare2 but with less, larger rolls (n≈8 and λ=2400 m), which also increases the transport of momentum per roll. The contrast can be explained by the stronger surface momentum fluxes in ECUME and WASP compared to the COARE and ANDREAS parameterizations (Figure 2a).

To assess the impact of the different parameterizations on horizontal and vertical winds in the middle of the boundary-layer and near the surface, Figure 8 shows probability density functions at 400 m, where convective rolls begin to form, and at 10 m. As in the reference simulation, Ecume2 and Wasp2 show narrow distributions

of vertical wind speeds at z=400 m (Figure 8a). The standard deviation values of 0.9 in Coare2 and 0.7 m s^{-1} in Ecume2 and Wasp2 indicate moderate vertical motion. Andreas2 shows a broader distribution and a standard deviation of 1.5 m s^{-1} with a peak shifted towards negative velocities. This shows higher variability in vertical velocities, marked by more pronounced upward and downward motions. At z=400 m, the horizontal wind speed is lower in Andreas2 compared to the other parameterizations, with a mean value of 46 instead of 47 m s^{-1} (Figure 8b). The slower wind is explained by the enhanced downward transport of momentum at this altitude. Near the surface, the distribution of wind speeds differs between the simulations. For Coare2, wind speeds are relatively low and this is consistent with the strong surface fluxes of momentum with the COARE parameterization. In contrast, they are significantly higher in Andreas2, averaging 3 m s^{-1} more than in Coare2. This difference can be explained by the more intense transport in Andreas2 (Figure 8c), which thus largely compensates for the strong surface momentum fluxes with the ANDREAS parameterization (Figure 2).

In summary, the increase in heat fluxes due to sea spray led to a more important thermal instability at the air-sea interface. This instability generates more intense vertical circulations in the boundary layer, leading to the formation of more and smaller convective rolls, over a larger vertical extent than in the reference simulation. As a result, momentum transport to the surface increases significantly, leading to stronger surface wind speeds than those found with other parameterizations.

4.3 Individual contribution of surface fluxes

The findings presented in the previous section suggest that surface heat fluxes contribute significantly to the organization of convective rolls and surface winds in combination with surface momentum fluxes. This section focuses on the NoH, NoLE and NoM simulations to determine the role of each kind of turbulent flux separately from the others. Without latent heat flux (NoLE), the boundary layer organization into convective rolls (Figures 9c and 9d) is similar to that of Coare2 (Figures 9a and 9b). In the absence of sensible heat flux (NoH), strong wind speeds in the form of a large packet are confined between z=250 m and a lower boundary layer height of around z=500 m (Figures 9e and 9f). The boundary layer is devoid of alternating upward and downward motions. This is due to reduced heating of the surface layer, which is typically responsible for convection and thus affect vertical motion. Without momentum flux (NoM), the wind speed is strongly enhanced (higher locally than 55 m s^{-1}) and disorganized, reaching lower levels because friction forces are not taken into account (Figures 9g and 9h).

The evolution of roll morphological parameters in Coare2, NoH, NoLE and NoM is evaluated every minute for the full 30-min duration of the simulations to assess their persistence in response to surface fluxes. The elliptical shape of the coherent structures is retained over time in Coare2 with a flatness parameter f superior to 0.7 (Figure 10a). The difference between wind and structure directions does not exceed 20° (Figure 10b). Overall, characteristic roll sizes fluctuate between 2000 and 3000 m, with an average of around 2100 m over 30 min (Figure 10c). Note that roll sizes are calculated with an accuracy of 200 m, i.e., the resolution of the simulations. The NoLE simulation shows a similar evolution for all parameters, albeit with a modest deviation from Coare2, particularly at 1530 UTC. Convective rolls in NoLE are on average slightly larger than in Coare2 with a size of around 2300 m. The divergences from the reference simulation are immediately apparent in NoM, whereas they appear after about 5 min in NoH. In both simulations, the flatness parameter tends towards very low values, and the structures become misaligned with the wind direction. Given that characteristic sizes are defined for structures with a

flatness parameter greater than 0.7, the ACF indicates that there is no spatial periodicity in the vertical velocity field. Consequently no roll structures are present after a few minutes of simulation.

Vertical wind speed profiles in the NoH and NoLE simulations are comparable to the reference simulation Coare2, with a slightly sharper decrease toward the surface in NoH (Figure 11a). In contrast, the NoM profile remains clearly distinct, with high wind speeds remaining almost uniform in the lower boundary layer. Unlike NoLE, which shows a decrease with height in virtual potential temperature in the first levels similar to Coare2, NoH is distinguished by a profile that maintains an almost constant virtual potential temperature, reflecting a nearly neutral atmosphere (Figure 11b). The instability parameter ζ tends to zero in that case, implying that shear is the main source of turbulence in the boundary layer (Table 2). ζ is no longer relevant in NoM. A value of ζ=0.50 in NoLE, as in Coare2, suggests that latent heat fluxes have weak impact on atmospheric instability and therefore on the formation of convective rolls. Although stability conditions are comparable, the momentum transport is somewhat weaker in NoLE (Figure 11c). This is attributed to the slightly higher roll size in NoLE, which results in fewer rolls in the region. In NoH, resolved fluxes remain limited compared to the Coare2 simulation and result in lower total transport, particularly at altitudes below 400 m where convective roll structures are more pronounced in the reference simulation. Moreover, turbulence becomes dominant in transport at higher altitude than in Coare2. Finally, the vertical transport profile in NoM is completely different from other simulations and vanishes near the surface due to the absence of momentum fluxes.

In short, the absence of sensible heat flux results in nearly neutral atmospheric conditions, inhibiting convection and hence the formation of convective rolls even in the presence of strong winds and intense shear. Consequently, momentum transport is considerably reduced, and is mainly controlled by subgrid-scale fluxes. Likewise, without momentum fluxes, wind shear is impacted, rapidly slowing down the formation of rolls. However, in the absence of latent heat fluxes, the convective rolls characteristics remain similar to the reference simulation.

5 Conclusions

Ensuring an accurate representation of air-sea fluxes is crucial to a better understanding of the marine atmospheric boundary layer dynamics. However, uncertainties persist in the parameterization of fluxes during windstorms, due to the lack of observations for wind speeds above 20 m s^{-1}. Such strong winds occurred during the passage of the Mediterranean cyclone Adrian studied here. The main objective of this study is to investigate the role of air-sea fluxes in the formation of fine-scale convective rolls using large eddy simulations (LES) run with the Meso-NH atmospheric model. Convective rolls, rarely studied in mid-latitude windstorms, have been shown to be involved in the downward transport of strong winds and the formation of maximum surface wind gusts associated with Adrian.

First, the impact of four air-sea flux parameterizations on mesoscale windstorm development is examined, using convection-permitting simulations over a period of 6-hours. The parameterizations used differ in the formulation of surface fluxes of latent heat, sensible heat and momentum, and also in the way they take into account the effects of physical processes such as sea spray. The choice of surface flux parameterization does not affect the windstorm trajectory. This shows that, on this relatively short time scale covering the mature phase of cyclogenesis, the windstorm trajectory is mostly driven by the large-scale flow. However, the windstorm intensity shows a slight sensitivity to the inclusion of sea spray effects in heat fluxes, which

reinforce heat fluxes. As a result, surface pressure drops by a few hPa more than in the other simulations, leading to a slight increase in surface wind speed.

Second, the impact of the four parameterizations on the development and organization of the convective rolls is examined through LES performed at a horizontal grid spacing of 200 m. Convective rolls are systematically formed in the strong wind region due to dynamic and thermal instabilities, whatever the air-sea flux parameterization used. A schematic (Figure 12) summarizes the main results relative to the sensitivity of convective rolls to surface fluxes. When heat fluxes are moderate, rolls are characterized by sizes of around 2000 m and extend vertically to the middle of the boundary layer (Figure 12, left panel). However, the morphological characteristics of the rolls are significantly influenced by surface fluxes, in particular the increased heat fluxes resulting from sea spray. Stronger heat fluxes lead to more important thermal instability at the air-sea interface. Hence, convection-induced vertical motions become more pronounced in the boundary layer. The convective rolls formed in such conditions are of reduced size, greater in number, and exhibit a higher vertical extent (Figure 12, middle panel). With this organization, the vertical transport of momentum by the convective rolls is increased by 40% and persists closer to the surface, before turbulence takes over. This results in higher surface wind speeds, although surface momentum fluxes are also strengthened by sea spray. This increase in vertical momentum transport approximately matches the increase in roll number, which leaves the transport per roll unaltered. Hence, it is assumed that the transport in the presence of sea spray is enhanced by the larger number of rolls. Furthermore, the stronger atmospheric instability results in a deeper boundary layer. This allows the rolls to form over a wider vertical extent and, consequently, to transport additional momentum from higher altitudes.

Third, the respective role of surface latent heat, sensible heat and moment fluxes is disentangled by performing LES sensitivity tests. Even in the absence of latent heat flux, convective rolls continue to form and retain similar characteristics, although their size is slightly affected. This indicates that latent heat fluxes have little impact on roll organization. In contrast, convective rolls quickly disappear without sensible heat fluxes (Figure 12, right panel). They also disorganize within a few minutes without surface momentum fluxes. Both of these fluxes are directly responsible for the combination of thermal and dynamic instability required to form and maintain convective rolls.

As shown in previous studies (Li et al., 2021; Lfarh et al., 2023), a large-scale simulation approach is indispensable for understanding the fine-scale processes responsible for transporting strong winds to the surface, such as the convective rolls in this study. The findings here highlight that, despite sufficient resolution to resolve such processes, an incomplete representation of the physical mechanisms at the air-sea interface under strong wind conditions can lead to significant discrepancies, which can have an impact on wind forecast and, consequently, on the safety of people and property.

The contribution of additional surface processes other than sea spray might be considered in future work. Although foam is regularly observed at the air-sea interface in strong winds, experiments to measure its impact on surface fluxes are relatively recent (Sroka & Emanuel, 2021). The role of foam in convective rolls and surface winds should be assessed and probably a contribution to consider in improving surface flux parameterizations. Apart from the turbulent exchange of air-sea fluxes, wind-wave interactions modify atmospheric and oceanic conditions, which can impact winds during windstorms. Considering the dynamic effects of waves can lead to improved forecasting of wind speeds in storms (Wahle et al., 2017). A first task for further studies is to couple the atmospheric model with a wave model. While surface latent heat exchange does not appear to be crucial for the development of

convective rolls, another approach would be to investigate the impact of cloud microphysics, focusing on the effect of evaporative cooling on roll formation and wind transport. It has been shown that evaporative cooling can reduce the buoyancy of air parcels in windstorms, facilitating their descent to the surface and contributing to the amplification of surface wind gusts (Browning et al., 2015; Ludwig et al., 2015).

In this study, all available data, including in-situ observations and satellite images, are exploited to evaluate the different simulations. However, when it comes to winds at sea, these data proved insufficient. Measurements from buoys at sea are lacking in the region of strong winds, and would be extremely useful for completing the validation of the simulations. Although large eddy simulations provide detailed information on fine-scale processes, their evaluation is hampered by the lack of high-resolution observations. In this context, synthetic aperture radar (SAR) satellite images have potential to reveal the details of convective rolls, as demonstrated by Brilouet et al. (2023); Stopa et al. (2022). Such observation may constrain parameterizations of surface fluxes via their control on roll characteristics. Thus, the methodology of LES over large domain developed here should be extended to other case studies. This would be essential to reach more general conclusions about the impact of air-sea fluxes on the transport of strong winds to the surface.

Appendix A Description of the turbulent flux parameterizations

The Coupled Ocean–Atmosphere Response Experiment (COARE3.0) (Fairall et al., 2003) used in the reference simulations, is one of the most commonly used parameterizations for interactions at the air-sea interface. COARE3.0 is derived from the COARE2.6 algorithm (Fairall et al., 1996) initially developed from observations made during the TOGA COARE experiment in the North Pacific (Webster & Lukas, 1992). COARE3.0 uses a new formulation for roughness length which slightly increases the fluxes for wind speeds above 10 m s^{-1}. The wave effect is taken into account through the roughness length. However, COARE3.0 is mainly valid for wind speeds up to 20 m s^{-1} due to the lack of observations for strong wind conditions.

ANDREAS (Andreas et al., 2015) is the only parameterization that distinguishes two different contributions to turbulent heat fluxes: standard air-sea interfacial fluxes and spray fluxes controlled by microphysical processes around the spray droplets. The small droplets are ejected into the atmosphere by bubble bursting at the air-sea interface during wave breaking or by the wave clipping mechanism of strong winds (Veron, 2015). The contribution to heat exchange becomes significant for wind speeds above 13 m s^{-1}. The total flux in the presence of sea spray is therefore the sum of the interfacial flux calculated by the bulk method and the flux related to sea spray calculated using the microphysical algorithm described in Andreas (2005).The ANDREAS parameterization was developed with observations including wind speeds up to 25 m s^{-1}.

ECUME6 is the new version of Exchange Coefficient Unified Multi-campaign Experiments. This parameterization is developed and used operationally by Météo-France (Belamari, 2005). ECUME6 is based on in-situ measurements of ocean-atmosphere fluxes from different field campaigns, considering strong wind conditions. Contrary to the COARE algorithms, the turbulent exchange coefficients are computed directly from the observations, which makes it impossible to take into account the effect of waves explicitly in the roughness length calculation. In ECUME6, measurements realized by Powell et al. (2003), Donelan et al. (2004) and French et al. (2007) allowed to consider the saturation and decrease of the exchange coefficients for wind speeds higher than 30 m s^{-1}.

WASP (Wave-Age Stress dependant Parametrization) (Sauvage et al., 2020) is based on the Coare3.0 and Coare3.5 parameterizations and allows wave growth to be explicitly taken into account in the calculation of roughness length in a wind range between 5 and 20 m s^{-1}. Above 20 m s^{-1}, the contribution of wave breaking is dominant, so wave age is no longer a sufficient parameter to represent the effect of sea state on surface roughness. Since different mechanisms are involved at low, moderate and high wind speeds, a piecewise continuous description is adopted to describe the Charnock parameter that relates waves and wind stress as a function of sea state. This approach makes it possible to represent the observed decrease in drag coefficient under intense wind conditions.

Acknowledgments

Computer resources for running Meso-NH were allocated by CALMIP through project P20024 and GENCI through project 0111437. This work was supported by the French National Research Agency under grant agreement ANR-21-CE01-0002 and by COST Action CA19109. The authors thank Carlos Granero Belinchon for providing the auto-correlation tools and for the discussions that contributed to the elaboration of a part of the paper and Météo France for making the in-situ observations available online through the MeteoNet application `https://meteonet.umr-cnrm.fr/`. The authors also thank Juan Escobar and Joris Pianezze of the Meso-NH support team for their assistance during this study.

References

Andreas, E. L. (2005). Approximation formulas for the microphysical properties of saline droplets. *Atmos. Res.*, *75*(4), 323–345. doi: 10.1016/j.atmosres.2005.02.001

Andreas, E. L., Mahrt, L., & Vickers, D. (2015). An improved bulk air–sea surface flux algorithm, including spray-mediated transfer. *Q. J. Roy. Meteorol. Soc.*, *141*(687), 642–654. doi: 10.1002/qj.2424

Atkinson, B. W., & Wu Zhang, J. (1996). Mesoscale shallow convection in the atmosphere. *Rev. Geophys.*, *34*(4), 403–431. doi: 10.1029/96RG02623

Belamari, S. (2005, 01). Report on uncertainty estimates of an optimal bulk formulation for surface turbulent fluxes. *MERSEA IP Deliverable 412*, 1–29.

Booth, J. F., Thompson, L., Patoux, J., & Kelly, K. A. (2012). Sensitivity of midlatitude storm intensification to perturbations in the sea surface temperature near the gulf stream. *Mon. Weather Rev.*, *140*(4), 1241–1256. doi: 10.1175/MWR-D-11-00195.1

Brilouet, P.-E., Bouniol, D., Couvreux, F., Ayet, A., Granero-Belinchon, C., Lothon, M., & Mouche, A. (2023). Trade wind boundary layer turbulence and shallow precipitating convection: New insights combining SAR images, satellite brightness temperature, and airborne in situ measurements. *Geophys. Res. Lett.*, *50*(2), e2022GL102180. doi: 10.1029/2022GL102180

Browning, K., Smart, D., Clark, M., & Illingworth, A. (2015). The role of evaporating showers in the transfer of sting-jet momentum to the surface. *Q. J. Roy. Meteorol. Soc.*. doi: 10.1002/QJ.2581

Brunke, M. A., Fairall, C. W., Zeng, X., Eymard, L., & Curry, J. A. (2003). Which bulk aerodynamic algorithms are least problematic in computing ocean surface turbulent fluxes? *J. Climate*, *16*(4), 619–635. doi: 10.1175/1520-0442(2003)0162.0.CO;2

Cavaleri, L., Bajo, M., Barbariol, F., Bastianini, M., Benetazzo, A., Bertotti, L., ... Umgiesser, G. (2019, 08). The October 29, 2018 storm in Northern Italy – An exceptional event and its modeling. *Prog. Oceanogr.*, *178*, 102178. doi: 10.1016/j.pocean.2019.102178

Chen, Y., Yuan, H., & Gao, S. (2019). A high-resolution simulation of roll convection over the Yellow Sea during a cold air outbreak. *J. Geophys. Res. Atmos.*, *124*(20), 10608-10625. doi: 10.1029/2019JD030968

Cuxart, J., Bougeault, P., & Redelsperger, J.-L. (2000). A turbulence scheme allowing for mesoscale and large-eddy simulations. *Q. J. Roy. Meteorol. Soc.*, *126*(562), 1–30. doi: 10.1002/qj.49712656202

Davolio, S., Fera, S. D., Laviola, S., Miglietta, M. M., & Levizzani, V. (2020). Heavy precipitation over Italy from the Mediterranean storm "Vaia" in October 2018: Assessing the role of an atmospheric river. *Mon. Weather Rev.*, *148*(9), 3571–3588. doi: 10.1175/MWR-D-20-0021.1

Donelan, M. A., Haus, B. K., Reul, N., Plant, W. J., Stiassnie, M., Graber, H. C., ... Saltzman, E. S. (2004). On the limiting aerodynamic roughness of the ocean in very strong winds. *Geophys. Res. Lett.*, *31*(18). doi: 10.1029/2004GL019460

Emanuel, K. (2003). A similarity hypothesis for air–sea exchange at extreme wind speeds. *J. Atmos. Sci.*, *60*(11), 1420–1428.

Etling, D., & Brown, R. A. (1993, August). Roll vortices in the planetary boundary layer: A review. *Bound. Layer. Meteor.*, *65*(3), 215–248. doi: 10.1007/BF00705527

Fairall, C. W., Bradley, E. F., Hare, J. E., Grachev, A. A., & Edson, J. B. (2003). Bulk parameterization of air–sea fluxes: Updates and verification for the coare algorithm. *J. Climate*, *16*(4), 571–591. doi: 10.1175/1520-0442(2003)0162.0.CO;2

Fairall, C. W., Bradley, E. F., Rogers, D. P., Edson, J. B., & Young, G. S. (1996). Bulk parameterization of air-sea fluxes for tropical ocean-global atmosphere coupled-ocean atmosphere response experiment. *J. Geophys. Res.*, *101 (C2)*(C2), 3747–3764. doi: 10.1029/95JC03205

Flamant, C. (2003). Alpine lee cyclogenesis influence on air-sea heat exchanges and marine atmospheric boundary layer thermodynamics over the western mediterranean during a tramontane/mistral event. *J. Geophys. Res.*, *108*(C2). doi: 10.1029/2001JC001040

Foster, R. C. (2005). Why rolls are prevalent in the hurricane boundary layer. *J. Atmos. Sci.*, *62*(8), 2647–2661. doi: 10.1175/JAS3475.1

French, J. R., Drennan, W. M., Zhang, J. A., & Black, P. G. (2007). Turbulent fluxes in the hurricane boundary layer. part i: Momentum flux. *J. Atmos. Sci.*, *64*(4), 1089–1102. doi: 10.1175/JAS3887.1

Giovannini, L., Davolio, S., Zaramella, M., Zardi, D., & Borga, M. (2021, 01). Multi-model convection-resolving simulations of the October 2018 Vaia storm over Northeastern Italy. *Atmos. Res.*, *253*, 105455. doi: 10.1016/j.atmosres.2021.105455

Granero Belinchon, C., Roux, S. G., Garnier, N. B., Tandeo, P., Chapron, B., & Mouche, A. (2022). Two-dimensional structure functions for characterizing convective rolls in the marine atmospheric boundary layer from Sentinel-1 SAR images. *Remote Sens. Lett.*, *13*(9), 946–957. doi: 10.1080/2150704X.2022.2112107

Gryschka, M., & Raasch, S. (2005). Roll convection during a cold air outbreak: A large eddy simulation with stationary model domain. *Geophys. Res. Lett.*, *32*(14). doi: 10.1029/2005GL022872

Jansà, A., Genoves, A., Picornell, M., Campins, J., Radinovic, D., & Alpert, P. (1994). Mediterranean cyclones: Subject of a wmo project. *The Life Cycle of Extratropical Cyclones*, *2*, 26–31.

Jeong, D., Haus, B. K., & Donelan, M. A. (2012). Enthalpy transfer across the air–water interface in high winds including spray. *J. Atmos. Sci.*, *69*(9), 2733–2748. doi: 10.1175/JAS-D-11-0260.1

Khanna, S., & Brasseur, J. G. (1998). Three-dimensional buoyancy- and shear-

induced local structure of the atmospheric boundary layer. *J. Atmos. Sci.*, *55*(5), 710–743. doi: 10.1175/1520-0469(1998)0552.0.CO;2

Lac, C., Chaboureau, J.-P., Masson, V., Pinty, J.-P., Tulet, P., Escobar, J., ... Wautelet, P. (2018). Overview of the Meso-NH model version 5.4 and its applications. *Geosci. Model Dev.*, *11*, 1929-1969. doi: 10.5194/gmd-11-1929-2018

Lewis, H. W., Castillo Sanchez, J. M., Arnold, A., Fallmann, J., Saulter, A., Graham, J., ... Clark, J. (2019). The ukc3 regional coupled environmental prediction system. *Geosci. Model Dev.*, *12*(6), 2357–2400. doi: 10.5194/gmd-12-2357-2019

Lfarh, W., Pantillon, F., & Chaboureau, J.-P. (2023). The downward transport of strong wind by convective rolls in a mediterranean windstorm. *Mon. Weather Rev.*. doi: 10.1175/MWR-D-23-0099.1

Li, X., Pu, Z., & Gao, Z. (2021). Effects of roll vortices on the evolution of hurricane harvey during landfall. *J. Atmos. Sci.*, *78*(6), 1847–1867. doi: 10.1175/JAS-D-20-0270.1

Liu, W. T., Katsaros, K. B., & Businger, J. A. (1979). Bulk parameterization of air-sea exchanges of heat and water vapor including the molecular constraints at the interface. *J. Atmos. Sci.*, *36*(9), 1722–1735. doi: 10.1175/1520-0469(1979)0362.0.CO;2

Lohou, F., Druilhet, A., & Campistron, B. (1998, January). Spatial and temporal characteristics of horizontal rolls and cells in the atmospheric boundary layer based on radar and in situ observations. *Bound. Layer. Meteor.*, *89*(3), 407-444. doi: 10.1023/A:1001791408470

Lohou, F., Druilhet, A., Campistron, B., Redelsperger, J. L., & Saïd, F. (2000, December). Numerical study of the impact of coherent structures on vertical transfers in the atmospheric boundary layer. *Bound. Layer. Meteor.*, *97*(3), 361-383. doi: 10.1023/A:1002641728075

Ludwig, P., Pinto, J. G., Hoepp, S. A., Fink, A. H., & Gray, S. L. (2015, April). Secondary Cyclogenesis along an Occluded Front Leading to Damaging Wind Gusts: Windstorm Kyrill, January 2007. *Mon. Weather Rev.*, *143*(4). doi: 10.1175/MWR-D-14-00304.1

Ludwig, P., Pinto, J. G., Reyers, M., & Gray, S. L. (2014). The role of anomalous sst and surface fluxes over the southeastern north atlantic in the explosive development of windstorm xynthia. *Q. J. Roy. Meteorol. Soc.*, *140*(682), 1729–1741. doi: 10.1002/qj.2253

Masson, V., Le Moigne, P., Martin, E., Faroux, S., Alias, A., Alkama, R., ... Voldoire, A. (2013, 07). The surfexv7.2 land and ocean surface platform for coupled or offline simulation of earth surface variables and fluxes. *Geosci. Model Dev.*, *6*, 929-960. doi: 10.5194/gmd-6-929-2013

Monin, A., & Obukhov, A. (1957). *Basic regularity in turbulent mixing in the surface layer of the atmosphere.* American Journal of Climate Change.

Morrison, I., Businger, S., Marks, F., Dodge, P., & Businger, J. A. (2005). An observational case for the prevalence of roll vortices in the hurricane boundary layer. *J. Atmos. Sci.*, *62*(8), 2662–2673. doi: 10.1175/JAS3508.1

Pergaud, J., Masson, V., Malardel, S., & Couvreux, F. (2009, July). A parameterization of dry thermals and shallow cumuli for mesoscale numerical weather prediction. *Bound. Layer. Meteor.*, *132*(1), 83-106. doi: 10.1007/s10546-009-9388-0

Perrie, W., Zhang, W., Andreas, E. L., Li, W., Gyakum, J., & McTaggart-Cowan, R. (2005). Sea spray impacts on intensifying midlatitude cyclones. *J. Atmos. Sci.*, *62*(6), 1867–1883. doi: 10.1175/JAS3436.1

Pineau-Guillou, L., Ardhuin, F., Bouin, M.-N., Redelsperger, J.-L., Chapron, B., Bidlot, J.-R., & Quilfen, Y. (2018). Strong winds in a coupled wave–atmosphere model during a north atlantic storm event: evaluation against observations. *Q. J. Roy. Meteorol. Soc.*, *144*(711), 317–332. doi:

10.1002/qj.3205

Powell, M., Vickery, P., & Reinhold, T. (2003, 04). Reduced drag coefficient for high wind speeds in tropical cyclones. *Nature*, *422*, 279–83. doi: 10.1038/nature01481

Richter, D. H., & Stern, D. P. (2014). Evidence of spray-mediated air-sea enthalpy flux within tropical cyclones. *Geophys. Res. Lett.*, *41*(8), 2997–3003.

Salesky, S. T., Chamecki, M., & Bou-Zeid, E. (2017, April). On the Nature of the Transition Between Roll and Cellular Organization in the Convective Boundary Layer. *Bound. Layer. Meteor.*, *163*(1), 41–68. doi: 10.1007/s10546-016-0220-3

Sauvage, C., Lebeaupin Brossier, C., Bouin, M.-N., & Ducrocq, V. (2020). Characterization of the air–sea exchange mechanisms during a Mediterranean heavy precipitation event using realistic sea state modelling. *Atmos. Chem. Phys.*, *20*(3), 1675-1699. doi: 10.5194/acp-20-1675-2020

Schultz, D. M., & Sienkiewicz, J. M. (2013). Using frontogenesis to identify sting jets in extratropical cyclones. *Wea. Forecasting*, *28*(3), 603–613. doi: 10.1175/WAF-D-12-00126.1

Shu, C.-W., & Osher, S. (1988, August). Efficient implementation of essentially non-oscillatory shock-capturing schemes. *J. Comput. Phys.*, *77*(2), 439–471. doi: 10.1016/0021-9991(88)90177-5

Sroka, S., & Emanuel, K. (2021). A review of parameterizations for enthalpy and momentum fluxes from sea spray in tropical cyclones. *Journal of Physical Oceanography*, *51*(10), 3053–3069. doi: 10.1175/JPO-D-21-0023.1

Sroka, S., & Emanuel, K. (2022). Sensitivity of sea-surface enthalpy and momentum fluxes to sea spray microphysics. *J. Geophys. Res.*, *127*(1), e2021JC017774. doi: 10.1029/2021JC017774

Stopa, J. E., Wang, C., Vandemark, D., Foster, R., Mouche, A., & Chapron, B. (2022). Automated global classification of surface layer stratification using high-resolution sea surface roughness measurements by satellite synthetic aperture radar. *Geophys. Res. Lett.*, *49*(12), e2022GL098686. doi: 10.1029/2022GL098686

Veron, F. (2015). Ocean spray. *Annu. Rev. Fluid Mech.*, *47*(1), 507–538. doi: 10.1146/annurev-fluid-010814-014651

Veron, F., Hopkins, C., Harrison, E. L., & Mueller, J. A. (2012). Sea spray spume droplet production in high wind speeds. *Geophys. Res. Lett.*, *39*(16). doi: 10.1029/2012GL052603

Wahle, K., Staneva, J., Koch, W., Fenoglio-Marc, L., Ho-Hagemann, H., & Stanev, E. V. (2017). An atmosphere–wave regional coupled model: improving predictions of wave heights and surface winds in the southern north sea. *Ocean Science*, *13*(2), 289–301. doi: 10.5194/os-13-289-2017

Webster, P. J., & Lukas, R. (1992). Toga coare: The coupled ocean–atmosphere response experiment. *Bull. Amer. Meteo. Soc.*, *73*(9), 1377–1416. doi: 10.1175/1520-0477(1992)0732.0.CO;2

Weckwerth, T. M., Horst, T. W., & Wilson, J. W. (1999). An observational study of the evolution of horizontal convective rolls. *Mon. Weather Rev.*, *127*(9), 2160–2179. doi: 10.1175/1520-0493(1999)127%3C2160:AOSOTE%3E2.0.CO;2

Zhao, B., Qiao, F., Cavaleri, L., Wang, G., Bertotti, L., & Liu, L. (2017). Sensitivity of typhoon modeling to surface waves and rainfall. *J. Geophys. Res.*, *122*(3), 1702–1723. doi: 10.1002/2016JC012262

Zou, Z., Zhao, D., Tian, J., Liu, B., & Huang, J. (2018). Drag coefficients derived from ocean current and temperature profiles at high wind speeds. *Tellus A: Dynamic Meteorology and Oceanography*, *70*(1), 1–13. doi: 10.1080/16000870.2018.1463805

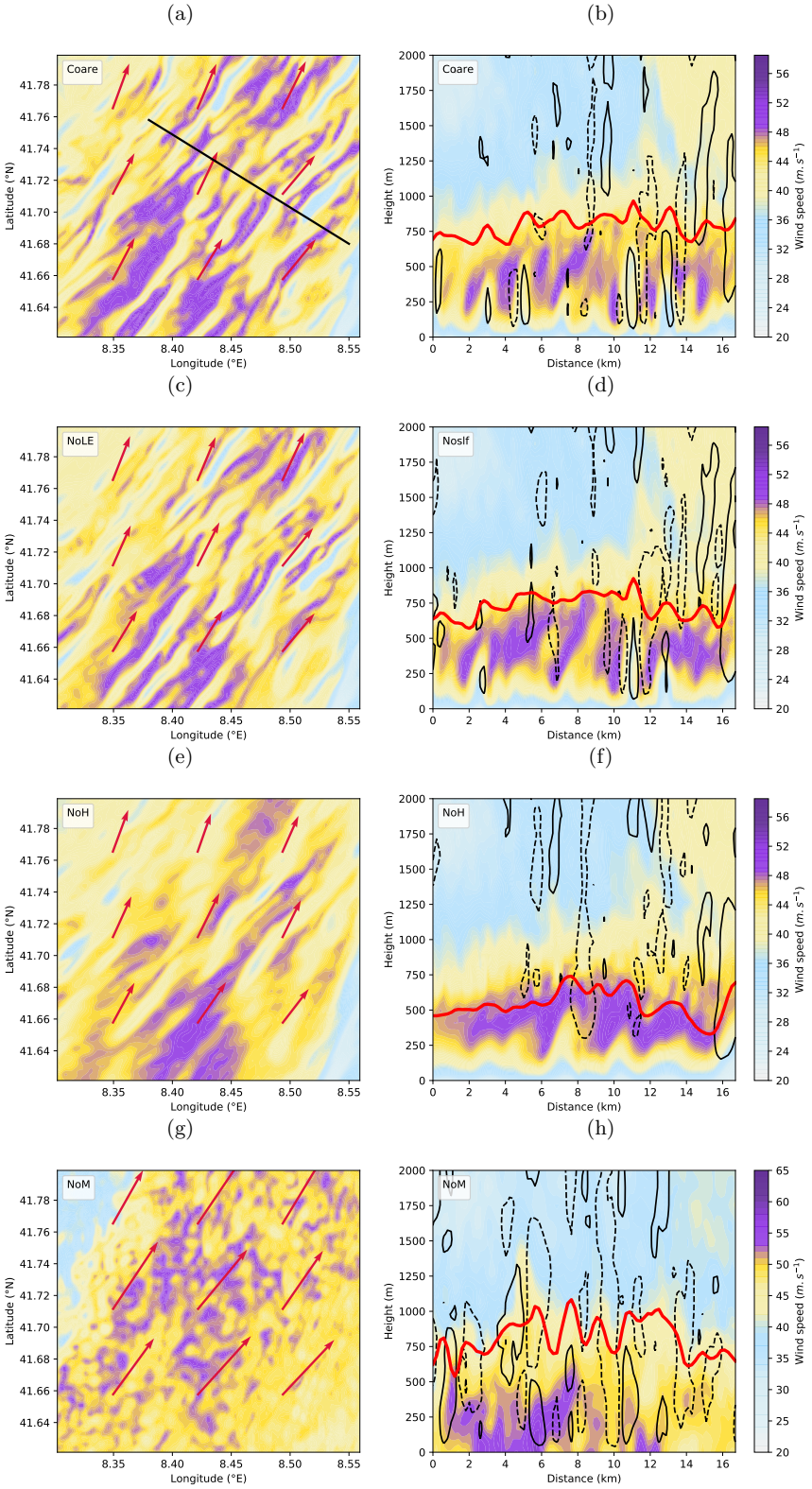

Figure 9: As in Figure 5, for (a, b) Coare2 (c, d) NoLE, (e, f) NoH and (g, h) NoM. For clarity, the color bar of wind speeds is scaled differently in NoM.

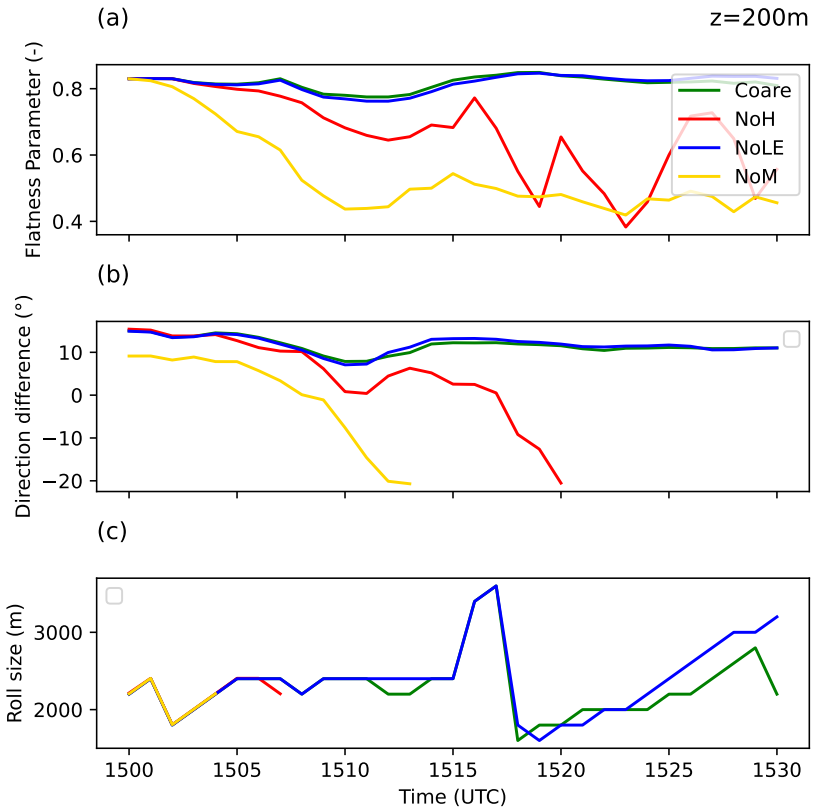

Figure 10: Temporal evolution of (a) flatness parameter, (b) direction and (c) structure size at z=200 m, for Coare2 (green), NoH (red), NoLE (blue) and NoM (gold).

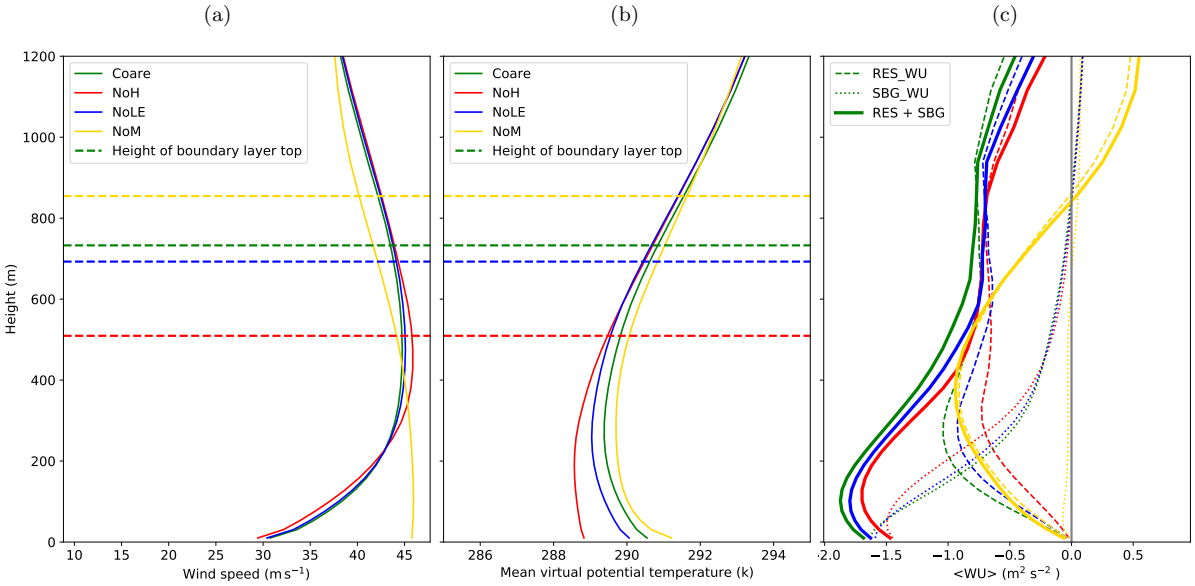

Figure 11: As in Figure 7, for Coare2, NoH, NoLE and NoM.

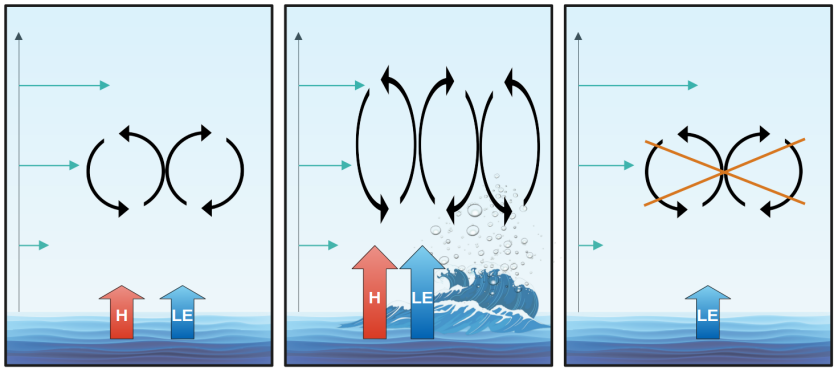

Figure 12: Summary of the main results of the paper. Red and blue vertical arrows represent surface sensible and latent heat fluxes, respectively, while green horizontal arrows represent the background wind shear and circling arrows represents convective rolls. See text for details.